Pergamon

Int. J. Heat Mass Transfer. Vol. 37, No. 6, pp. 939–954, 1994

0017-9310/94 $6.00+0.00

0017-9310(93)E0019-D

Analysis of dispersion effects and non-thermal equilibrium, non-Darcian, variable porosity incompressible flow through porous media

A. AMIRI and K. VAFAI

Department of Mechanical Engineering, The Ohio State University, Columbus, OH 43210, U.S.A.

(*Received* 6 *May* 1993 *and in final form* 11 *October* 1993)

Abstract—The present work involves the numerical simulation of forced convective incompressible flow through porous media, and the associated transport processes. A full general model for the momentum equation was employed. The mathematical model for energy transport was based on the two-phase equation model which assumes no local thermal equilibrium between the fluid and the solid phases. The investigation aimed at a comprehensive analysis of the influence of a variety of effects such as the inertial effects, boundary effects, porosity variation effects, thermal dispersion effects, validity of local thermal equilibrium assumption and two dimensionality effects on the transport processes in porous media. The results presented in this work provide detailed yet readily accessible error maps for assessing the importance of various simplifying assumptions which are commonly used by researchers.

1. INTRODUCTION

THE TRANSPORT phenomena in porous media have been of continuing interest for the past five decades. This interest stems from the complicated and interesting phenomena associated with transport processes in porous media. The wide applications available have led to numerous investigations in this area. Such applications can be found in solar receiver devices, building thermal insulation, heat exchangers, energy storage units, ceramic processing and catalytic reactors to name a few. Utilization of porous layers for transpiration cooling by water for fire fighting and rescue operations has also proved to be a promising research area. Yano *et al.* [1] have experimentally investigated the utilization of porous layers and water to maintain low temperature even in fire conditions. This is important for a number of applications such as security systems and safety equipment which demand thermal protection in the initial stage of a fire. Our attention in this study focuses on packed beds of solid sphere particles in particular and porous media in general.

Many aspects in this field are important to explore for a thorough understanding of the fluid mechanics and the heat transfer characteristics that are involved in the transport phenomena through porous beds. Some of the aspects related to transport phenomena were tackled in the literature. Vafai and Tien [2] discussed the potential of the inertial effects and the solid boundary effects on momentum and energy transport through constant-porosity media. The investigation provided insight on the applicability of the customarily employed Darcy's law.

In some applications, such as drying and metal processing, the constant-porosity assumption is invalid. It has been recognized that an impermeable boundary influences the porosity distribution of a porous medium. The porosity is high in the vicinity of an impermeable boundary and decreases to an asymptotic value at about four to five sphere diameters from it. Moreover, the porosity of the bed was found to exhibit sinusoidally damping decay especially close to the wall (Roblee *et al.* [3] and Benenati and Brosilow [4]). This phenomenon introduces the channeling effect which has been widely discussed in the literature [5–12].

An important topic in packed beds relates to the mixing and recirculation of local fluid streams as the fluid flows through tortuous paths offered by the solid particles. This secondary flow effect is classified as thermal dispersion. Extensive attention has been given to studies on the determination of the axial and radial effective thermal conductivities in cylindrical packed beds [13–17]. Investigations by Cheng and Vortmeyer [10] and Hunt and Tien [11] provided some insight into the physics of the dispersion phenomenon. The aforementioned work neglected the inertial effects from the proposed model. Previous investigations [18–20] have noted the small contribution from the axial dispersion to the overall energy transport and the fact that its significance is confined to low Peclet or particle Reynolds numbers. This is because the convective heat transfer dominates the axial diffusion mode at high flow rates, therefore, the axial dispersion quantity can be neglected without causing significant impact on the heat transfer results. Subsequent analytical models, such as those cited by Hunt and Tien [11] and Cheng and Zhu [21], were proposed to simulate the energy transport in porous media. These models have taken into consideration the non-Darcian effects and the thermal dispersion effects. However, variations do exist among these models in terms of the Nusselt number predictions at various

NOMENCLATURE

a_1, a_2 porosity variation parameters, equation (12)
a_{sf} specific surface area of the packed bed [m^{-1}]
c_p specific heat at constant pressure [$J\ kg^{-1}\ K^{-1}$]
d_p particle diameter [m]
dp/dx pressure gradient [$N\ m^{-3}$]
Da Darcy number, K_x/H^2
F the geometric function defined in equation (6)
h_{sf} fluid-to-solid heat transfer coefficient [$W\ m^{-2}\ K^{-1}$]
H height of the packed bed [m]
i index for x-coordinate
j index for y-coordinate
J unit vector oriented along the pore velocity vector, $v_p/|v_p|$
k thermal conductivity [$W\ m^{-1}\ K^{-1}$]
K permeability [m^2]
L length of the pack bed [m]
LTE local thermal equilibrium
Nu Nusselt number
Pr Prandtl number, $\mu C_{p_f}/k_f$
Re_p particle Reynolds number, $\rho_f u_c d_p/\mu$
t time [s]
T temperature [K]
u velocity component in the x-direction [$m\ s^{-1}$]
v velocity vector [$m\ s^{-1}$]
x, y Cartesian coordinates [m].

Greek symbols
α thermal diffusivity [$m^2\ s^{-1}$]
γ shape parameter defined in equation (22)
ε porosity
η dimensionless vertical scale defined in equation (21)
θ dimensionless fluid phase temperature, $(T_w - T_f)/(T_w - T_{m_f})$
Θ dimensionless solid phase temperature, $(T_w - T_s)/(T_w - T_{m_s})$
μ dynamic viscosity [$kg\ m^{-1}\ s^{-1}$]
ξ dimensionless length scale defined in equation (23)
ρ density [$kg\ m^{-3}$]
ω relaxation factor for successive over relaxation scheme.

Subscripts
e inlet
f fluid
feff effective property for fluid
m mean
o reference
s solid
seff effective property for solid
w wall
x x-component
y y-component
∞ asymptotic or free stream.

Superscripts
f fluid
s solid
* dimensionless quantity.

Symbols
$\langle\ \rangle$ 'local volume average' of a quantity.

Peclet numbers due to incorporating different formulations for the porosity variation and the effective thermal conductivity [22].

In all the above mentioned investigations, a single-phase model was adopted which assumes a state of local thermal equilibrium (LTE) between the fluid and the solid phase at any location in the bed. This is a common practice for most of the investigations in this area where the temperature gradient at any location between the two phases is assumed to be negligible. This assumption must be relaxed for a number of problems such as fixed bed nuclear propulsion systems and nuclear reactor modeling where the temperature difference between the coolant and the solid rods becomes crucial. Recent investigation by Vafai and Sözen [23], which was based on the two-phase equation model, reported significant discrepancies between the fluid and solid phase temperature distributions. The investigation by Vafai and Sözen [23] allowed a simple characterization scheme for interpreting the applicability of LTE condition and the one dimensional approach for various compressible flow conditions and porous bed configurations.

To our knowledge, the investigations performed to date for establishing adequate models for transport phenomena in porous media with incompressible working fluids incorporate one or more simplifying assumptions such as LTE condition, neglect of the axial conduction term from the energy equation, one dimensional approach, constant porosity assumption and neglect of boundary and inertial effects. In the present work, the steady-state analysis of incompressible flow through a bed of uniform solid sphere particles packed randomly is discussed. Pertinent velocity and temperature fields are presented. Different effects such as the inertial effect, the macroscopic shear stress (solid boundary effect) and the effect of the porosity variation model on the momentum and energy transport in a confined porous bed are discussed. Moreover, the inclusion of thermal dis-

persion effects on the convective energy transport in packed beds are discussed in great detail. Finally, the LTE assumption and the two dimensionality behavior are illustrated in integrated forms. The percentage error involved in calculating the Nusselt number between the generalized model, which incorporates all non-Darcian effects and simplified models which lack one or more of the non-Darcian effects are illustrated in terms of error maps. These error maps allow a simple characterization scheme for interpreting the applicability of the simplified models to various flow conditions and bed configurations. Throughout the analysis, the choice of three non-dimensional parameters is found to be inherently tied to the physics of the problem. These parameters are the particle Reynolds number, the Darcy number and the solid-to-fluid diffusivity ratio.

2. ANALYSIS

The problem under investigation is forced convection of incompressible fluid flow through a packed bed of spherical particles as illustrated in Fig. 1(a). The computational length and height of the bed were chosen to be 50 and 20 cm, respectively. The extent of the packed bed in the z-direction is assumed to be long enough that the problem will essentially be two dimensional.

At this point it is instructive to summarize the assumptions on which the established model is based.

(1) The medium is isotropic. However, the dependency of quantities such as the geometric function and the effective thermal conductivities are accounted for.

(2) The solid spheres are of uniform shape and incompressible.

(3) The forced convection dominates the packed bed, i.e. natural convection effects are negligible.

(4) The variation of thermophysical properties with temperature is ignored. This is a reasonable assumption for the operating temperature range applied (40 K) in the analysis.

(5) Due to the relatively low operating temperature considered in the present study, the inter-particle and intra-particle radiation heat transfer are neglected.

2.1. *Governing equations*

By assimilating the above points, the system of the governing equations can be presented in the following vectorial form based on the volume average technique [2, 7, 23]:

Continuity equation

$$\nabla \cdot \langle v \rangle = 0 \tag{1}$$

Momentum equation

$$\frac{\rho_f}{\varepsilon}\langle (v\cdot\nabla)v\rangle = -\frac{\mu}{K}\langle v\rangle - \frac{\rho_f F\varepsilon}{\sqrt{K}}[\langle v\rangle\cdot\langle v\rangle]J + \frac{\mu}{\varepsilon}\nabla^2\langle v\rangle - \nabla\langle P\rangle^f \tag{2}$$

Fluid phase energy equation

$$\varepsilon\langle\rho_f\rangle^f c_{p_f}\frac{\partial\langle T_f\rangle^f}{\partial t} + \langle\rho_f\rangle^f c_{p_f}\langle v\rangle\cdot\nabla\langle T_f\rangle^f = \nabla\cdot\{k_{feff}\cdot\nabla\langle T_f\rangle^f\} + h_{sf}a_{sf}(\langle T_s\rangle^s - \langle T_f\rangle^f) \tag{3}$$

Solid phase energy equation

$$(1-\varepsilon)\rho_s c_{p_s}\frac{\partial\langle T_s\rangle^s}{\partial t} = \nabla\cdot\{k_{seff}\cdot\nabla\langle T_s\rangle^s\} - h_{sf}a_{sf}(\langle T_s\rangle^s - \langle T_f\rangle^f) \tag{4}$$

where $\langle\psi_\alpha\rangle^\alpha$ refers to the intrinsic phase average of quantity ψ for phase α. The physical aspects of various terms in the governing equations are discussed in refs. [2, 7, 23] and the symbols are defined in the nomenclature. It is important to know that the time interval within which steady-state condition is reached for the velocity field is of the order of a few seconds for most practical cases (Vafai and Tien [24]). Therefore, in the numerical analysis the steady-state forms of the continuity and the momentum equations, equations (1) and (2), are considered.

The permeability of the packed bed and the geometric function are based on experimental results [25] and may be expressed in the following form [7]:

$$K = \frac{\varepsilon^3 d_p^2}{150(1-\varepsilon)^2} \tag{5}$$

$$F = \frac{1.75}{\sqrt{(150)\varepsilon^{3/2}}} \tag{6}$$

where d_p is the particle diameter. The specific surface area of the packed bed which appears in both energy equations, equations (3) and (4), is developed based on geometrical considerations (Vafai and Sözen [23]):

$$a_{sf} = \frac{6(1-\varepsilon)}{d_p}. \tag{7}$$

The formulation of the fluid-to-solid heat transfer coefficient in this study was based on an empirical correlation established by Wakao *et al.* [15, 16] and is presented as follows

$$h_{sf} = k_f\left[2 + 1.1Pr^{1/3}\left(\frac{\rho u d_p}{\mu}\right)^{0.6}\right]\Big/ d_p. \tag{8}$$

In the present study, the dispersion phenomenon is treated as an additional diffusive term added to the stagnant component (Hunt and Tien [11]). The stagnant component is expressed in terms of the phase porosities and the individual thermal conductivities of the phases. The empirical correlation developed by Wakao and Kaguei [16] is employed in this study to model the effective conductivities.

$$(k_{feff})_x = \varepsilon k_f + 0.5\left[Pr\left(\frac{\rho u d_p}{\mu}\right)\right]k_f \tag{9}$$

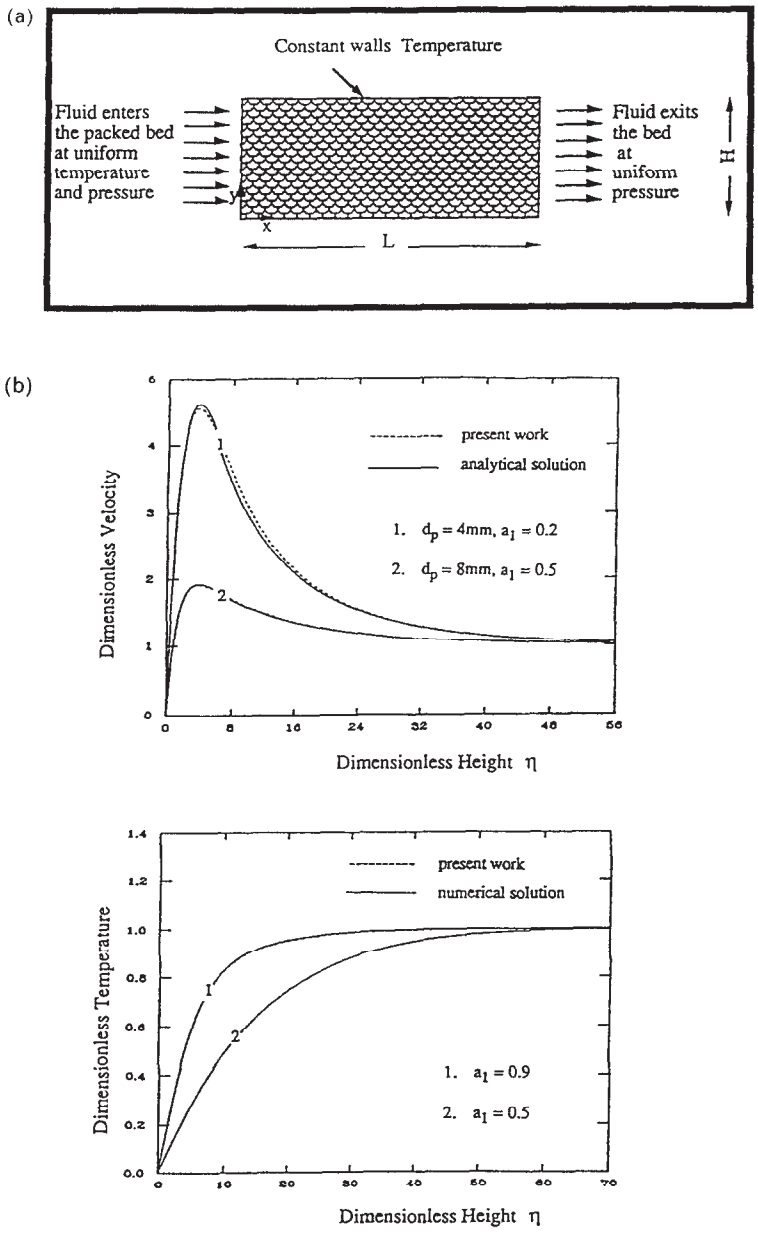

FIG. 1. (a) Schematic diagram of the problem. (b) Comparison of field variable distribution of the present work against the analytical and the numerical solutions of Vafai [9].

$$(k_{\text{feff}})_y = \varepsilon k_f + 0.1\left[Pr\left(\frac{\rho u d_p}{\mu}\right)\right]k_f \tag{10}$$

$$k_{\text{seff}} = (1-\varepsilon)k_s. \tag{11}$$

As mentioned earlier, experimental observations [3, 4] indicate that the porosity in a randomly packed bed is functionally dependent on the distance from the wall. A common practice is to consider an exponential decaying function to approximately simulate the porosity variation. This can be expressed mathematically as

$$\varepsilon = \varepsilon_\infty\left[1 + a_1 \exp\left(\frac{-a_2 y}{d_p}\right)\right] \tag{12}$$

where ε_∞ is the free stream porosity while a_1 and a_2 are empirical constants. The free steam porosity was chosen to be 0.37, whereas $a_1 = 1.7$ and $a_2 = 6$. These values were found to be a good approximation to the above reported experimental data [3, 4]. Moreover, these constants will be utilized in the computations wherever the exponential porosity model is used.

The porosity variation can be more rigorously pre-

dicted by accounting for the damped oscillation close to the wall. A model proposed by Mueller [26] was found to closely simulate the experimental finding of Benenati and Brosilow [4]. Since the exponential decaying function ignores the damped oscillation, the proposed model will display how far the exponential function is from the 'actual' porosity variation model given by Mueller [26].

The Nusselt number is separately defined for the fluid and solid phase and is expressed as

Fluid phase Nusselt number

$$Nu_f = -\frac{2H}{T_w - T_{m_f}}\left(\frac{\partial \langle T_f \rangle^f}{\partial y}\right)_{y=0} \tag{13}$$

Solid phase Nusselt number

$$Nu_s = -\frac{2H}{T_w - T_{m_s}}\left(\frac{\partial \langle T_s \rangle^s}{\partial y}\right)_{y=0} \tag{14}$$

where T_{m_f} and T_{m_s} are the mixed mean temperature of the fluid and the solid phase respectively and are defined as follows

$$T_{m_f} = \frac{\int_0^H u\, T_f \, dy}{U_m H} \tag{15}$$

$$T_{m_s} = \frac{\int_0^H T_s \, dy}{H}. \tag{16}$$

It should be mentioned that the definition of the Nusselt number essentially represents the temperature gradient at the boundary. This was purposely done since studies in the literature define the Nusselt number in a similar manner even for a variable conductivity medium. However, the error maps, presented in Figs. 3 and 6, are established based on the heat flux condition, i.e. after multiplying the Nusselt number, as given by equations (13) and (14), by k_{eff} so that the enhancement in heat flux can be accounted for when transverse dispersion is considered.

2.2. *Boundary conditions*

In the problem under investigation, the no slip boundary condition is imposed at the wall and the walls are kept at constant temperature. The boundary conditions are, therefore, as follows

$$u(x, y = 0) = u(x, y = H) = 0 \tag{17}$$

$$T_f(x, y = 0) = T_s(x, y = 0) = T_w \tag{18}$$

$$T_f(x, y = H) = T_s(x, y = H) = T_w \tag{19}$$

$$T_f(x = 0, y) = T_s(x = 0, y) = T_e. \tag{20}$$

The entrance and boundary temperatures were taken as:

$$T_e = 300 \text{ K}, \quad T_w = 340 \text{ K}.$$

Solid spherical particles of different sizes and materials were considered. Particle diameter values of 2, 5 and 8 mm were utilized in the computations. Several runs were also performed for a particle diameter of 6.4 mm. Different fluids were also considered to provide a broad range of solid-to-fluid diffusivity ratios. The Prandtl number was assumed constant for all the thermophysical properties. The Reynolds number was varied by applying different axial pressure gradients. The physical data for different fluid and solid phases which were considered in the numerical computations are calculated at the average film temperature and are presented in Table 1. These values were chosen as they are representative of some applications. It should be noted that the main features and conclusions obtained in this work are not dependent on the actual entrance or boundary temperature values.

3. SOLUTION METHODOLOGY

An explicit finite difference scheme was employed to solve the system of the governing equations subject to the cited boundary conditions. The numerical scheme was based on the finite difference versions of equations (1)–(4). The steady-state solutions of these equations were obtained. Variable grid size was implemented in the y-direction while the grid size in the x-direction was kept constant. A fine, equally spaced, grid size was positioned within 4% of the total height from each external boundary while a relatively coarser, equally spaced, grid size was used for the core region. Since the study under investigation pertains to forced convection, the momentum equation and the energy equations are not coupled. The momentum equation was handled by first linearizing the nonlinear term. The resulting set of algebraic equations was solved by tridiagonalization of the solution matrix.

The energy equations were handled in the following manner. The spatial derivatives were discretized by the central differencing except for the convective term which is approximated by an upwind differencing scheme. At grid points on the right boundary, a three point differencing was employed for the spatial x-derivatives instead of the Neumann (insulated) boundary conditions. This was achieved by linear extrapolation from the preceding two grid points in the x-direction. This assumption is valid since the problem under consideration has a strong parabolic behavior. The validity of the assumption was examined by extending the computational domain beyond the physical axial dimension. The computational length of the bed was systematically increased until the numerical results within the physical domain were no longer affected by an increase in the length of the computational domain.

The energy equations were solved for the fluid and

Table 1. Physical data

(a) Fluid phase

	Density, ρ_f (kg m^{-3})	Specific heat, C_{p_f} (J kg^{-1} K^{-1})	Thermal conductivity, k_f $\times 10^3$ (W m^{-1} K^{-1})	Viscosity, μ $\times 10^5$ (kg m^{-1} s^{-1})
Air	1.1	1008	28	1.9
Water	989	4180	640	57.7

(b) Solid phase

	Density, ρ_s (kg m^{-3})	Specific heat, C_{p_s} (J kg^{-1} K^{-1})	Thermal conductivity, k_s (W m^{-1} K^{-1})
Lead	7660	448	82
AISI304	7900	485	15.2
Soda Lime	2225	835	1.4

the solid phase temperature fields using the successive over relaxation scheme (SOR). The source term which is a function of the field temperature was updated after each iteration. The spatial derivative in the Nusselt number was computed by using three point differencing. The numerical computations were performed on a CRAY YMP/28. The accuracy of the numerical results was rigorously examined. Moreover, the stability of the numerical scheme has been tested by increasing the number of grid points in both directions to ensure a proper combination of Δx and Δy. A systematic decrease in the grid size was employed for obtaining grid independence results. It was assumed steady-state conditions have been reached when the temperature values for the fluid and the solid phase in two consecutive iterations differed by less than the convergence criterion of 10^{-10}.

4. RESULTS AND DISCUSSION

To examine the validity of the numerical scheme, the numerical results were compared with the most closely related analytical and numerical solutions. This was achieved by making the necessary adjustments to our model to reduce it to a system equivalent to the simplified available cases. Our numerical results for the velocity distribution were compared with the analytical results obtained by Vafai [9]. The analytical solution given by Vafai [9] had a restriction that $a_1 < 1$ for the solution to be valid. As no analytical solution was given for temperature distribution, the numerical results from Vafai [9] were used for such comparison. The physical properties for velocity distribution comparison were chosen as: (1) $dp/dx = 1493$ N m^{-3}, $d_p = 4$ mm, $\varepsilon_\infty = 0.3$, $a_1 = 0.2$, $a_2 = 2.0$ and (2) $dp/dx = 1493$ N m^{-3}, $d_p = 8$ mm, $\varepsilon_\infty = 0.3$, $a_1 = 0.5$, $a_2 = 2.0$. While the physical properties for the temperature distribution comparison were chosen as $dp/dx = 1.2 \times 10^5$ N m^{-3}, $d_p = 8$ mm, $\varepsilon_\infty = 0.4$ with the following empirical constants: (1) $a_1 = 0.9$, $a_2 = 2.0$ and (2) $a_1 = 0.5$, $a_2 = 2.0$. Figure 1(b) demonstrates such a comparison in terms of the dimensionless variables that appear in the work of Vafai [9]. As may be seen from Fig. 1(b), the comparisons display an excellent agreement.

The results from the computations will be presented in a non-dimensional form. The dimensionless velocity, fluid and solid phase temperature distributions chosen for presenting the results are defined as: $u^* = u/u_c$, $\theta = (T_w - T_f)/(T_w - T_{m_f})$ and $\Theta = (T_w - T_s)/(T_w - T_{m_s})$, respectively. Based on the analysis presented by Vafai and Tien [2], the velocity and the temperature fields are plotted against a dimensionless vertical scale, η, expressed as:

$$\eta = \frac{y\gamma_\infty}{\xi^{1/2}} \tag{21}$$

where γ_∞ is the free stream shape parameter and ξ, the dimensionless length scale and are defined as:

$$\gamma_\infty = \sqrt{\frac{\varepsilon_\infty}{K_\infty}} \tag{22}$$

$$\xi = x/L. \tag{23}$$

The velocity and temperature profiles are presented at $\xi = 0.5$. In addition, the local Nusselt number distributions for the two phases are plotted against ξ.

4.1. *Non-Darcian effects*

Figures 2(a) and (b) depict the non-Darcian effects on the velocity and temperature field distributions as well as the Nusselt number variations. The results shown are for the following physical values: $\alpha_s/\alpha_f = 25.6$, $Da = 1.36 \times 10^{-6}$, and $Re_p = 100$. The dispersion effects were incorporated in Fig. 2(a) while they are excluded from the results presented in Fig.

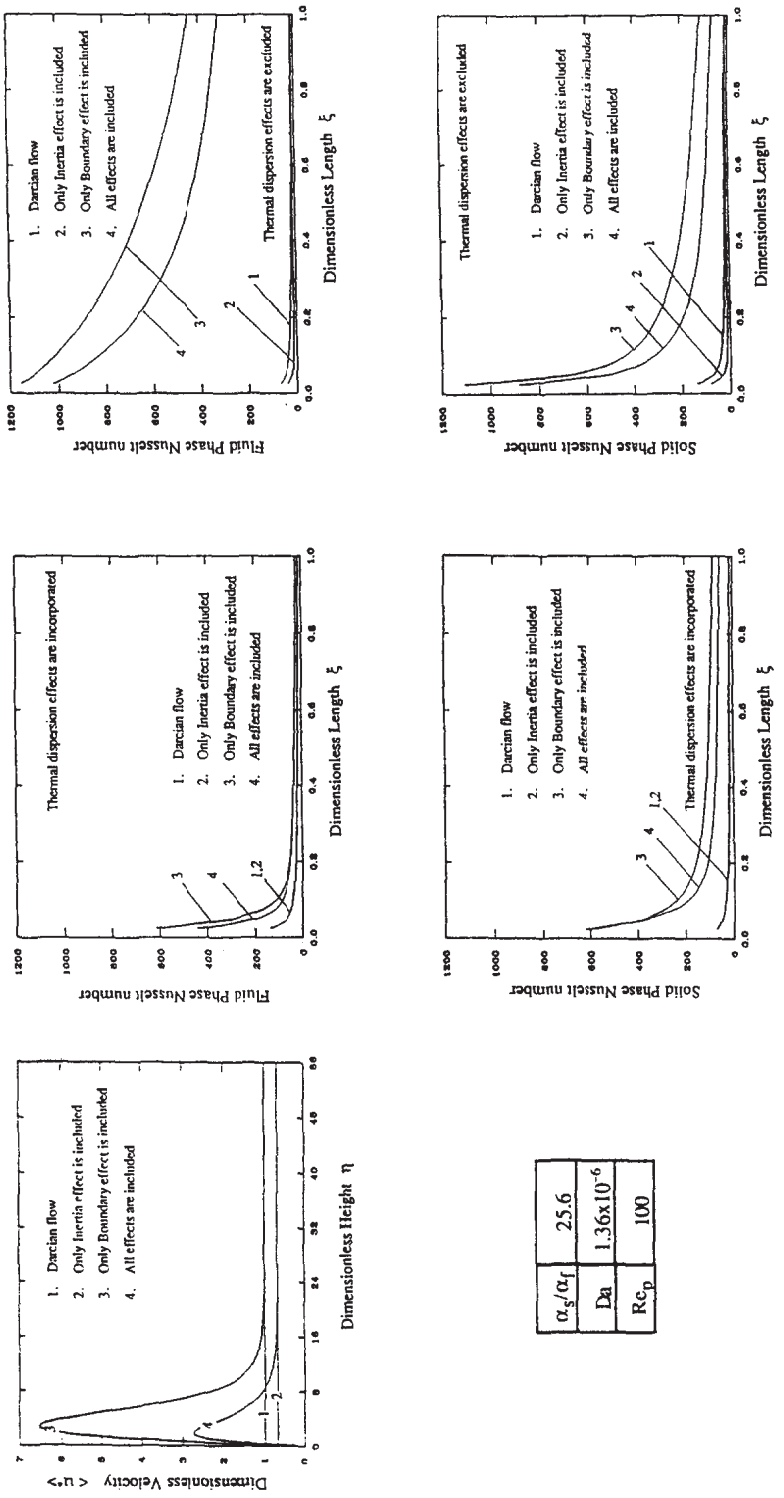

FIG. 2. Effect of the non-Darcian parameters on velocity field and Nusselt number distributions using the exponential porosity model for $\alpha_s/\alpha_f = 25.6$, $Da = 1.36 \times 10^{-6}$ and $Re_p = 100$, for (a) thermal dispersion effects incorporated, (b) thermal dispersion effects excluded.

2(b). As can be seen from Figs. 2(a) and (b), not accounting for the impermeable boundary reduces the velocity profile to a slug flow due to the absence of the shear stress along the boundary. In addition, cases 3 and 4 illustrate that omitting the inertia term in the momentum equation increases the velocity near the wall region as inertial effects introduce a further damping. In general, higher velocities cause an increase in the convected energy carried away from the boundary compared with that by conduction. This results in a thinner thermal boundary layer leading to an increase in the Nusselt number. It is important to recapitulate that the 'conventional' definition of the Nusselt number, as given by equations (13) and (14), is a measure of the temperature gradient at the boundary rather than the quantity of the heat flux generated when the variable conductivity medium is considered. As a result of defining the Nusselt number based on temperature gradient instead of the actual heat flux, the model that excludes the transverse dispersion effect exhibits a larger Nusselt number. However, it should be noted that the heat flux for the case when the dispersion is included is higher than when it is excluded.

To explore the non-Darcian effects for a wide range of Re_p and Da, an error map is presented for the average fluid phase Nusselt number. Taking the generalized model as a basis, comparisons with the values obtained by the other simplified models that neglect one or more non-Darcian effects were made for a given Re_p and Da. The percentage error involved in calculating the average fluid phase Nusselt number was found from

$$\% \text{ error} = \frac{|Nu(\text{simplified model}) - Nu(\text{generalized model})|}{Nu(\text{generalized model})} \times 100. \quad (24)$$

These comparisons are presented in Fig. 3. The thermal dispersion effects are incorporated in the depicted results. The results are presented for solid-to-fluid diffusivity ratio equal to 0.16, 4.87 and 25.6. The numbers in parentheses represent the errors in using the Darcy model, the modified-Darcy model (the Darcy model modified to account for the inertia) and the generalized model that neglects the inertial effect, respectively. That is, the first number in each entry represents the error in using the Darcy model as compared to the generalized model, the second number represents the error in using the modified Darcy model and the third entry represents the error in using the generalized model without the inertial effect as compared to the generalized model. It can be easily seen that as the Da and Re_p increase, the computed percentage error also increases. An exception for this is the error computed from using the Darcy model where the percentage error decreases as Re_p increases. This is because the average velocity computed from Darcy's law always increases by increasing the pressure gradient, thus, approaching the velocity computed from the generalized model. Consequently, the rate of convection predicted by the generalized model and the Darcy model follows each other closely as Re_p increases. Figure 3 clearly shows that significant error is encountered for most cases when employing any of the simplified models even for low Re_p and Da.

4.2. *The effect of the actual porosity variation*

Figure 4 depicts the effect of employing the 'actual' porosity variation model instead of the familiar exponential model. The dispersion effects were incorporated in Fig. 4(a) while they were excluded from the results presented in Fig. 4(b). The physical data were: $\alpha_s/\alpha_f = 4.87$, $Da = 5.32 \times 10^{-7}$, and $Re_p = 10$. The velocity profile is the most sensitive field variable to any variation in the porosity. Thus, the velocity profile is formed proportional to the porosity variation as shown in Fig. 4. The overall temperature distribution is not expected to vary remarkedly except in a confined region (close to the wall) in response to the variation in the velocity magnitude. Hence, the Nusselt number demonstrates a better choice of representation for the heat transfer rate. Employing the 'actual' porosity model reveals a different Nusselt number distribution from that when the exponential model is used. These effects are more pronounced when the dispersion effects are incorporated as the effective fluid conductivities depend on the velocity vector.

4.3. *Thermal dispersion effects*

The variation of the field variables for the case with $\alpha_s/\alpha_f = 4.87$, $Da = 5.32 \times 10^{-7}$ and $Re_p = 10$ are shown in Fig. 5. The velocity field is not shown since the influence of dispersion is confined to energy transport. The results show that the longitudinal dispersion has negligible effect in forming the overall thermal boundary layer. In addition, its effect may be unlikely to be detected even in terms of Nusselt number distribution. Figure 6 shows that the Nusselt number distribution for the model that incorporates dispersion is lower than the model that excludes dispersion effects in the transverse direction. The 'conventional' definition of the Nusselt number, defined in equations (13) and (14), which expresses merely the temperature gradient, fails to adequately present the enhancement in energy transport due to incorporating transverse dispersion effects. Thus, the Nusselt number results in the model that neglects transverse dispersion show an increase over the model that adopts dispersion. The enhancement due to dispersion effects becomes apparent once the temperature gradient is multiplied by the effective transverse thermal conductivity as given in equation (10) to obtain the actual quantity of the general heat flux. Therefore, the heat flux values for the case when the dispersion effects are included are indeed higher than when the dispersion effects are excluded.

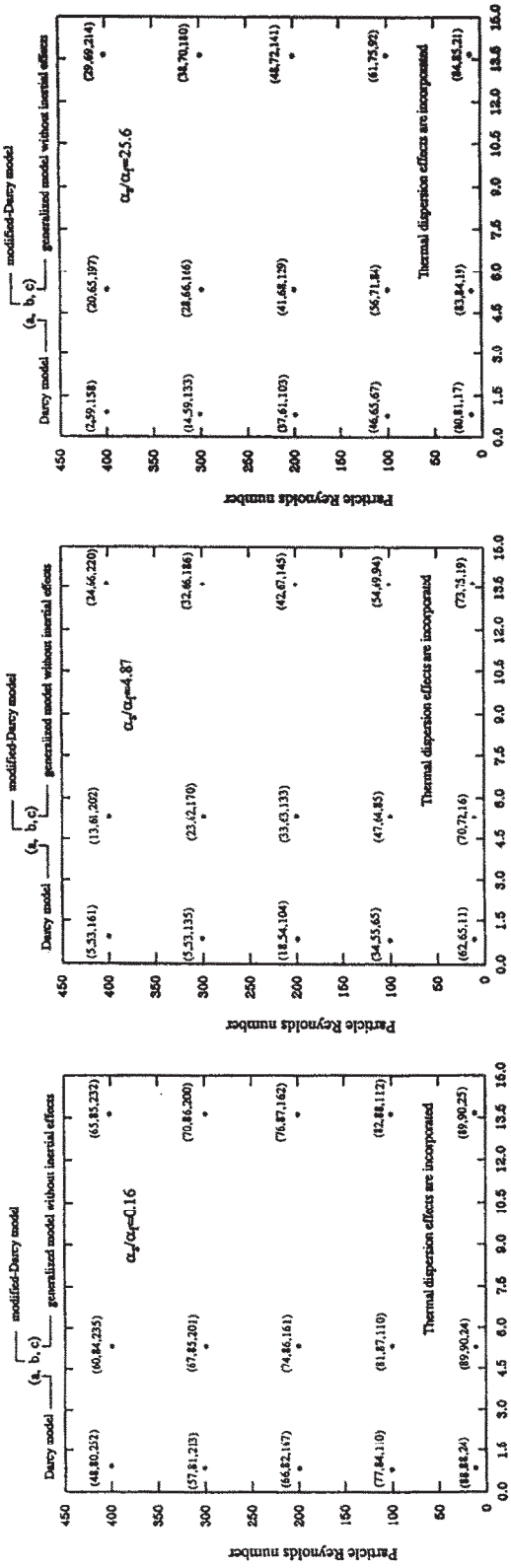

FIG. 3. The percent error on the average fluid Nusselt number using different simplified models in one or both coordinates while incorporating the exponential porosity model and the dispersion effects in all of the models for the cases with α_s/α_f equal to 0.16, 4.87 and 25.6.

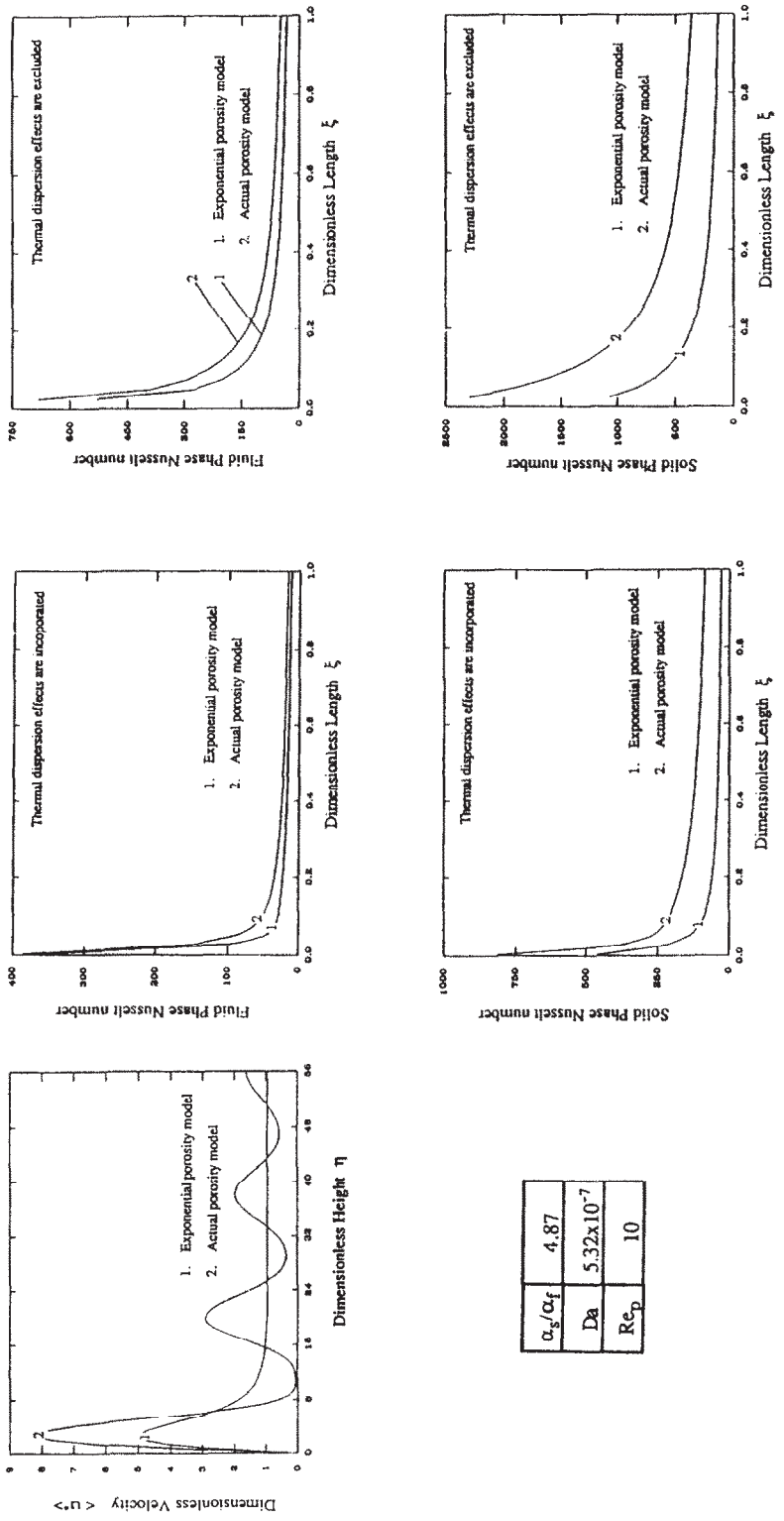

FIG. 4. Effect of the porosity variation model on Nusselt number distribution for $\alpha_s/\alpha_f = 4.87$, $Da = 5.32 \times 10^{-7}$ and $Re_p = 10$. for (a) thermal dispersion effects incorporated, (b) thermal dispersion effects excluded.

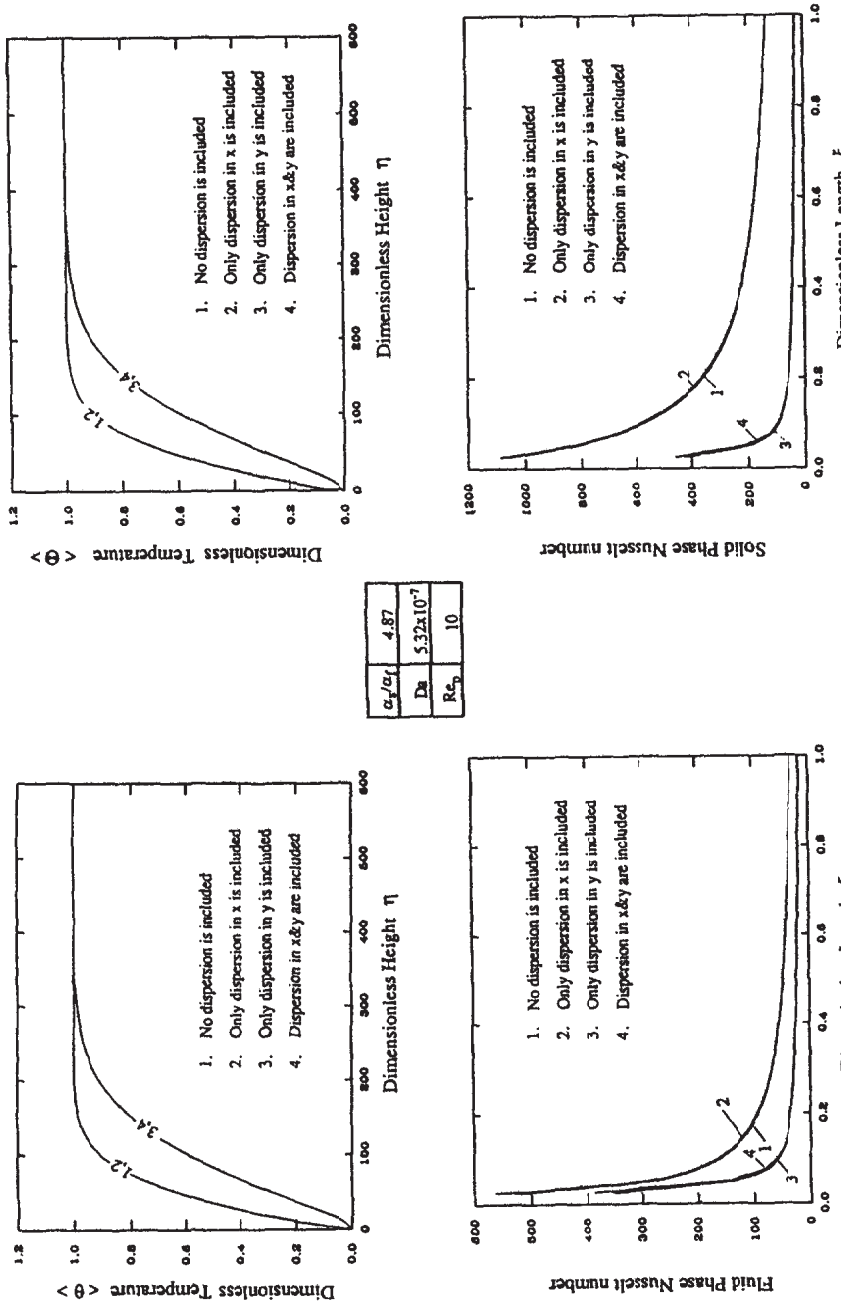

FIG. 5. Effect of thermal dispersion on the temperature fields and the Nusselt number distributions using the exponential porosity model for $\alpha_s/\alpha_f = 4.87$, $Da = 5.32 \times 10^{-7}$ and $Re_p = 10$.

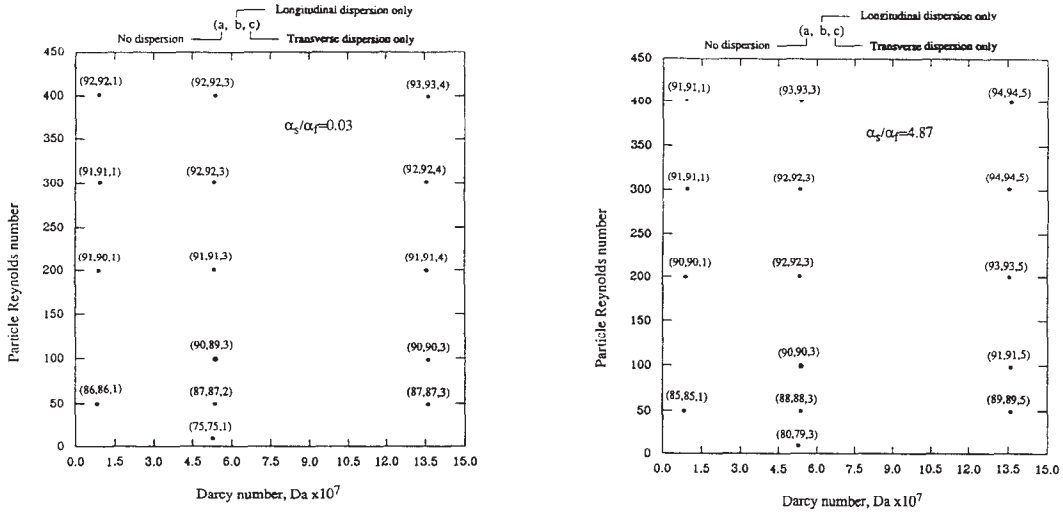

FIG. 6. The percent error on the average fluid Nusselt number for dropping the thermal dispersion effects in one or both coordinates while employing the exponential porosity model in all of the models for the cases with α_s/α_f equal to 0.03 and 4.87.

To examine the significance of the longitudinal and the transverse thermal dispersion effects more vigorously, an error map is established in terms of the average fluid phase Nusselt number to display the significance of dispersion effects in both directions for a wide range of Da and Re_p. The generalized model that incorporates the dispersion effects in both directions was used as the basis of comparison. The comparisons were carried out with simplified models that lack the dispersion effects in one or both directions. The average fluid phase Nusselt number was used for establishing the error map. To demonstrate the heat transfer augmentation due to dispersion effects, the Nusselt number was based on the actual heat flux which is imposed on the external boundary. The percentage error involved in calculating the average fluid phase Nusselt number was found from equation (24).

These comparisons are shown in Fig. 6 for solid-to-fluid diffusivity ratios equal to 0.03 and 4.87. The numbers between the parentheses represent the estimated error in dropping the dispersion effects in both directions, nomal direction and axial direction, respectively. That is, the first number in each entry represents the error in neglecting the dispersion in both directions as compared to the generalized model, whereas the second number represents the error in using the longitudinal dispersion only and the third entry represents the error in using the transverse dispersion as compared to the generalized model. Figure 6 shows that the Darcy number is the primary parameter, affecting the magnitude of the longitudinal dispersion. On the other hand, Fig. 6 confirms that the transverse dispersion plays the major role in the dispersion phenomenon in porous beds. This is because the thermal boundary layer growth is more dependent on the transverse thermal conductivity as compared to the axial thermal conductivity.

4.4. *Local Thermal Equilibrium (LTE) assumption*

The examination of LTE was carried out by comparing the temperature distributions of the fluid and solid phases locally, i.e. at each grid point. This may be expressed in the following form

$$\%\ \mathrm{LTE} = |\theta_{(i,j)} - \Theta_{(i,j)}| \times 100. \qquad (25)$$

To classify the outcome based on qualitative ratings for LTE assumption, the following categories were adopted: very good, less than 1%; good, 1–5%; fair, 5–10%; poor 10–15%, and very poor, more than 15%. It may seem from an overall view of the figures presented earlier for the fluid and solid temperature distribution that LTE assumption for steady-state incompressible flow is a fair one. However, a closer look at the temperature distributions near the wall region shows appreciable differences between the two phases. Figure 7 demonstrates such an assessment using the exponential porosity model for different thermal diffusivity ratios. It can be concluded from Fig. 7 that the Darcy number is the most influential parameter in determining the validity of local thermal equilibrium. The particle Reynolds number also plays a role in this regard. Based on Fig. 7, the local thermal equilibrium assumption becomes less pronounced as both Re_p and Da increase. In addition, the effect of the solid-to-fluid thermal diffusivity ratio in the dividing lines is obvious.

The 'actual' porosity model exhibits poor to very poor ratings in terms of LTE condition for the diffu-

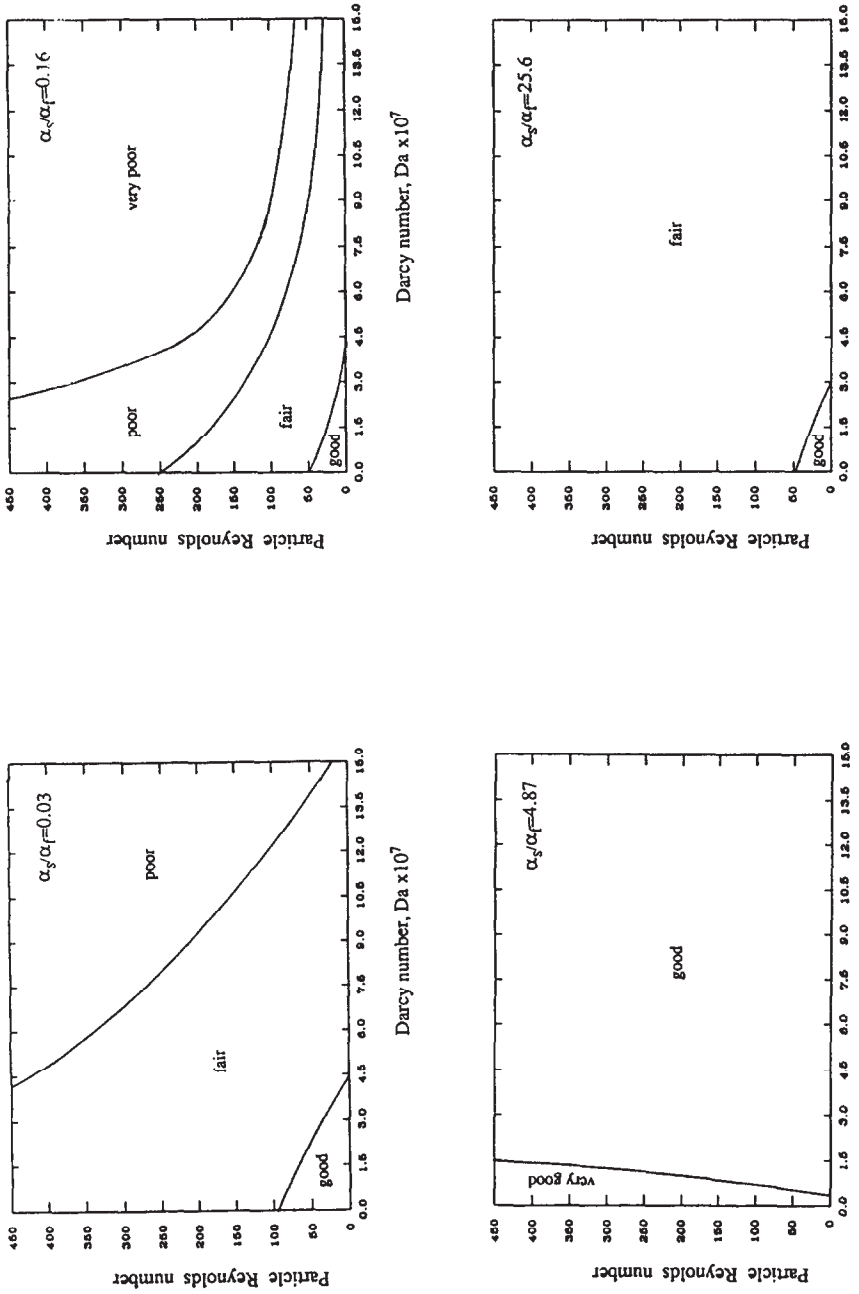

FIG. 7. Qualitative assessment for LTE for the cases with α_s/α_f equal to 0.03, 0.16, 4.87 and 25.6, respectively. (The exponential porosity model is employed and dispersion effects are incorporated.)

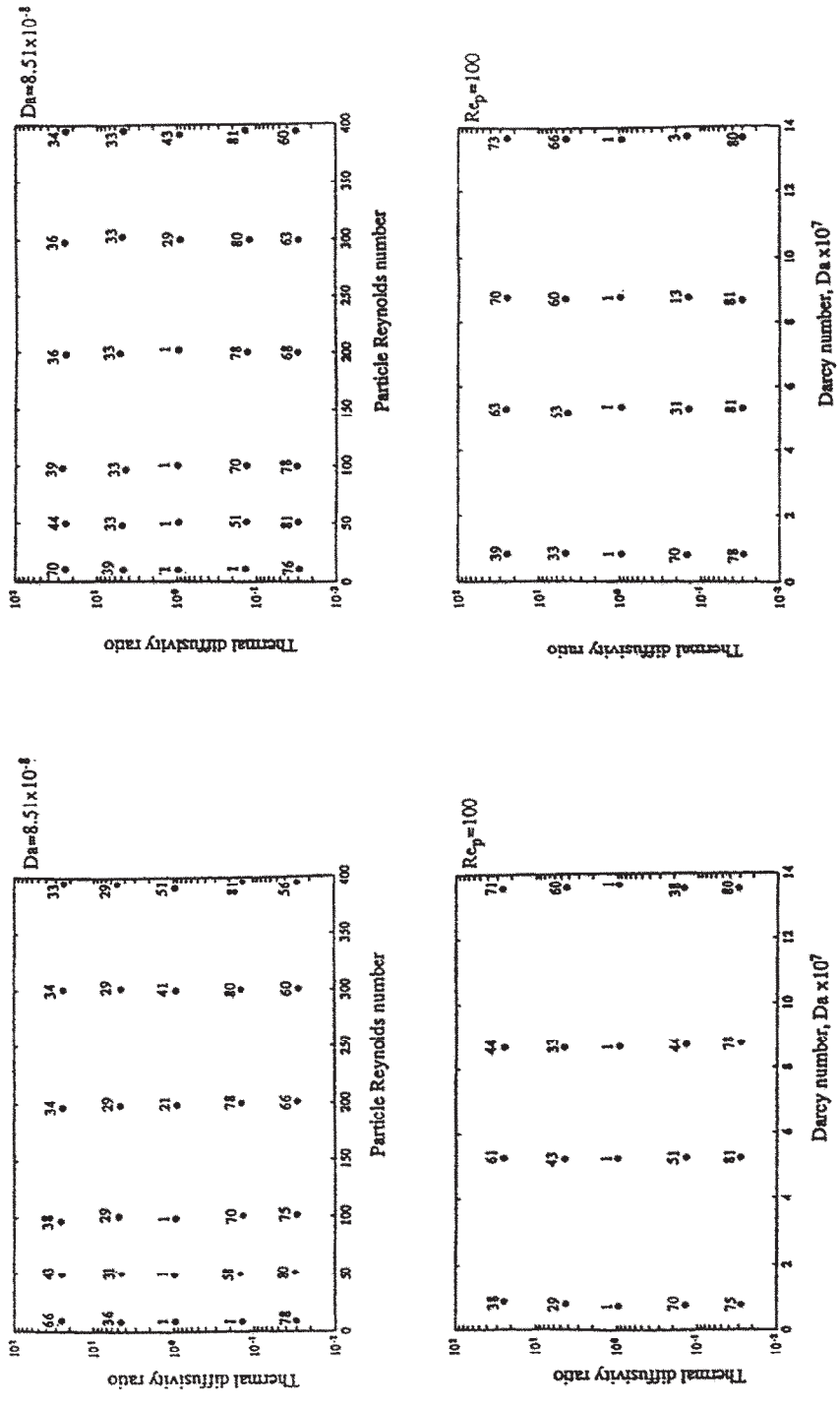

FIG. 8. Assessment of the strength of the two-dimensionality effects for the generalized model that incorporates dispersion effects using (a) the actual porosity model, (b) the exponential porosity model.

sivity ratios used. The higher level of convection obtained by employing the 'actual' porosity model in the region close to the wall increases the temperature difference between the fluid and the solid particles, thus, the ratings were found as such. For brevity, the results for the 'actual' porosity model are not shown here.

4.5. *The two-dimensionality behavior of packed beds*

In conjunction with the validity of LTE, a quantitative assessment for the strength of the two-dimensional behavior was conducted in a similar manner. The fluid and solid phase midplane temperatures at a selected section were compared with the fluid and solid phase local temperatures, respectively, along the same section. The end section of the packed bed was chosen since the thermal boundary layer reaches its maximum thickness at the end of the physical domain. The computational runs performed show very small variations in two-dimensionality behavior for each of the two phases. Therefore, for brevity, the results are presented for the fluid phase only. The assessment of the strength of the two-dimensional behavior was established in two steps. First, the difference between the dimensionless temperature of a local position and the midplane was computed from

$$\% \text{ difference} = |\theta(x = L, y) - \theta(x = L, y = H/2)|. \tag{26}$$

The difference was checked starting from the midplane location and moving downward. At each local normal position, the '% difference' cited in equation (26) was evaluated. The height at which the '% difference' between the local and midplane temperatures becomes equal to or greater than 2.5% was cited. The region beyond this height was considered to have significant two-dimensional effects. Next, the percent of the distance traveled (the spotted position) to half channel height was found from

$$\% \text{ height} = \frac{y(\text{located position})}{\text{half channel width}} \tag{27}$$

where y is measured from the bottom plate. The '% height' was set to be equal to the strength of the two-dimensionality of the packed bed for the given physical conditions. Thus, the higher '% height' reflects a stronger two-dimensional behavior. Figures 8(a) and (b) demonstrate the assessment of the strength of the two-dimensional behavior for the exponential and the 'actual' porosity variation models, respectively. For each porosity model the two-dimensionality characteristics are shown for two cases. First, for a fixed Da and a range of Re_p, and also for a fixed Re_p and a range of Da. Several interesting features are seen in these figures which invite further investigation in this area. A three-dimensional view could provide a better perspective for the two-dimensionality behavior as a function of α_s/α_f, Da and Re_p. However, such a three-dimensional figure was found to be less informative than the presented format.

5. CONCLUSIONS

In this work, accurate simulation of transport phenomena in packed beds has been accomplished. The analysis has been conducted for steady, incompressible forced convective fluid flow. In addition, the simulation was carried out using separate energy equations for the fluid and solid phases. Furthermore, the investigation aimed at exploring the influence of a variety of effects such as the inertial effects, the boundary effects, the porosity variation model and the thermal dispersion effects on the transport processes in packed beds. What is more, the validity of LTE condition and the two-dimensionality behavior were also presented. In addition, comprehensive error maps on the basis of the numerical findings have been presented. These error maps establish a characterization scheme for interpreting the applicability of the simplified models and various simplifying assumptions for various flow conditions and bed configurations.

Acknowledgement—The authors gratefully acknowledge the computer time provided by The Ohio Supercomputer Center for the numerical computations.

REFERENCES

1. T. Yano, M. Ochi and S. Enya, Protection against fire and high temperature by using porous media and water, *Pro. ASME/JSME Th. Engng* pp. 213–218 (1991).
2. K. Vafai and C. L. Tien, Boundary and inertia effects on flow and heat transfer in porous media, *Int. J. Heat Mass Transfer* **108,** 195–203 (1981).
3. L. H. S. Roblee, R. M. Baird and J. W. Tierney, Radial porosity variation in packed beds, *A.I.Ch.E. Jl* **8**(3), 359–361 (1958).
4. R. F. Benenati and C. B. Brosilow, Void fraction distribution in beds of spheres, *A.I.Ch.E. Jl* **4,** 450–464 (1962).
5. C. E. Schwartz and J. M. Smith, Flow distribution in packed beds, *Ind. Engng Chem.* **45,** 1209–1218 (1953).
6. B. C. Chadrasekhara and D. Vortmeyer, Flow model for velocity distribution in fixed porous beds under isothermal conditions, *Thermal Fluid Dyn.* **12,** 105–111 (1979).
7. K. Vafai, Convective flow and heat transfer in variable-porosity media, *J. Fluid Mech.* **147,** 233–259 (1984).
8. K. Vafai, R. L. Alkire and C. L. Tien, An experimental investigation of heat transfer in variable porosity media, *ASME J. Heat Transfer* **107,** 642–647 (1985).
9. K. Vafai, Analysis of the channeling effect in variable porosity media, *J. Energy Res. Technol.* **108,** 131–139 (1986).
10. P. Cheng and D. Vortmeyer, Transverse thermal dispersion and wall channeling in a packed bed with forced convective flow, *Chem. Engng Sci.* **43**(9), 2523–2532 (1988).
11. M. L. Hunt and C. L. Tien, Non-Darcian convection in cylindrical packed beds, *J. Heat Transfer* **110,** 378–384 (1988).
12. K. J. Renken and D. Poulikakos, Experiment and analysis of forced convection heat transport in a packed bed

of spheres, *Int. J. Heat Mass Transfer* **31**, 1399–1408 (1988).
13. S. Yagi and D. Kunii, Studies on effective thermal conductivities in packed beds, *A.I.Ch.E. Jl* **3**(3), 373–381 (1957).
14. S. Yagi and D. Kunii, Studies on heat transfer near wall surface in packed beds, *A.I.Ch.E. Jl* **61**(1), 97–104 (1960).
15. N. Wakao, S. Kaguei and T. Funazkri, Effect of fluid dispersion coefficients on particle-to-fluid heat transfer coefficients in packed beds, *Chem. Engng Sci.* **34,** 325–336 (1979).
16. N. Wakao and S. Kaguei, *Heat and Mass Transfer in Packed Beds*. Gordon and Breach, New York (1982).
17. J. Levec and R. G. Carbonell, Longitudinal and lateral thermal dispersion in packed beds, *A.I.Ch.E. Jl* **31**(4), 591–602 (1985).
18. D. J. Gunn and J. F. C. Desouza, Heat transfer and axial dispersion in packed beds, *Chem. Engng Sci.* **29,** 1363–1371 (1974).
19. D. Vortmeyer, Axial heat dispersion in packed beds, *Chem. Engng Sci.* **30,** 999–1001 (1975).
20. M. Sözen and K. Vafai, Longitudinal heat dispersion in porous beds with real gas flow, *J. Thermophys. Heat Transfer* **7**(1), 153–157 (1993).
21. P. Cheng and C. T. Zhu, Effect of radial thermal dispersion on fully-developed forced convection in cylindrical packed tubes, *Int. J. Heat Transfer* **30,** 2373–2383 (1987).
22. F. C. Chou, J. H. Su and S. S. Lien, A reevaluation of non-Darcian forced convection in cylindrical packed tubes. In *Fundamentals of Heat Transfer in Porous Media*, ASMEHTD—Vol. 193, pp. 57–66 (1992).
23. K. Vafai and M. Sözen, Analysis of energy and momentum transport for fluid flow through a porous bed, *J. Heat Transfer* **112,** 690–699 (1990).
24. K. Vafai and C. L. Tien, Boundary and inertia effects on convective mass transfer in porous media, *Int. J. Heat Mass Transfer* **25,** 1183–1190 (1982).
25. S. Ergun, Fluid flow through packed columns, *Chem. Engng Pro.* **48,** 89–94 (1952).
26. G. E. Mueller, Prediction of radial porosity distribution in randomly packed fixed beds of uniformly sized spheres in cylindrical containers, *Chem. Engng Sci.* **46,** 706–708 (1991).